PERGAMON

International Journal of Heat and Mass Transfer 42 (1999) 423–435

International Journal of HEAT and MASS TRANSFER

Analytical characterization and conceptual assessment of solid and fluid temperature differentials in porous media

Dae-Young Lee[a], Kambiz Vafai[b,*]

[a] *Korea Institute of Science and Technology, Seoul 130-650, Korea*
[b] *Department of Mechanical Engineering, The Ohio State University, Columbus, OH 43210, U.S.A.*

Received 25 February 1998; in final form 21 May 1998

Abstract

An analytical characterization of forced convective flow through a channel filled with a porous medium is presented in this work. Based on a two-equation model, including transverse conduction contributions, exact solutions are obtained for both fluid and solid phase temperature fields. The Nusselt number is also obtained in terms of the pertinent physical parameters, namely the Biot number for the internal heat exchange and the ratio of effective conductivities between the fluid and solid phases. It is shown that the heat transfer characteristics can be classified within three regimes, each of which is dominated by one of three distinctive heat transfer mechanisms, i.e., fluid conduction, solid conduction and internal heat exchange between solid and fluid phases. Based on these results, a complete electrical thermal network representative of transport through porous media is established. In addition, an analytical characterization and conceptual assessment of solid and fluid temperature differentials is presented, the validity of the one-equation model is investigated and a practical criterion is suggested for channels with different cross sections.

Nomenclature

a interfacial area per a unit volume of porous media [m^{-1}]
A_c cross-section area of the channel [m^2]
A_i interfacial area between solid and fluid phases [m^2]
A_w outer surface area of the porous medium [m^2]
Bi Biot number defined in equation (14)
c constants defined in equation (40)
c_P specific heat of the fluid [J kg^{-1} K^{-1}]
c_1, c_2 constants defined in equations (49) and (50)
D hydraulic diameter of the channel [m]
E error in the Nusselt number defined by equation (63)
E_a allowable error in the Nusselt number
h_i interstitial heat transfer coefficient [W m^{-2} K^{-1}]
h_w wall heat transfer coefficient defined by equation (23) [W m^{-2} K^{-1}]
H characteristic length of the channel [m]
$k_{f,eff}$ effective thermal conductivity of the fluid [W m^{-1} K^{-1}]
$k_{s,eff}$ effective thermal conductivity of the solid [W m^{-1} K^{-1}]
Nu_w Nusselt number defined by equation (24)
Nu_{wl} Nusselt number calculated from one-equation model
P perimeter of the channel [m]
q heat flux [W m^{-2}]
q_w heat flux at the wall [W m^{-2}]
R thermal resistance [m^2 K W^{-1}]
T temperature [K]
u fluid velocity [m s^{-1}]
$\bar{u}$ nondimensional velocity defined in equation (7)
V volume of the porous media filled in the channel [m^3]
x longitudinal coordinate [m]
y transverse coordinate [m].

Greek symbols

$\Delta\theta$ nondimensional temperature difference, $\Delta\theta = \theta_s - \theta_f$
ε porosity at the wall
η nondimensional transverse coordinate defined in equation (7)
γ geometric constant defined by equation (8)

* Corresponding author.

0017–9310/98 $19.00
PII: S0017–9310(98)00185–9

θ nondimensional temperature defined in equation (7)
κ ratio of the effective fluid conductivity to that of the solid, $= k_{f,eff}/k_{s,eff}$
λ parameter defined by equation (21)
ρ fluid density [kg m^{-3}].

Subscripts
f fluid or conduction in fluid phase
i internal heat exchange
o overall
s solid or conduction in solid phase
$\langle\rangle$ average over the channel cross section, $\langle f\rangle = \int_{A_c} f \mathrm{d}A_c/A_c$.

1. Introduction

Forced convective heat transfer in porous media has been a subject of continuing interest during the past decades. This interest is due to the wide range of applicability of heat transfer processes in porous media such as solar receiver devices, building thermal insulation, energy storage units, heat pipes and catalytic reactors. More recently, utilization of porous inserts has proved to be very promising in heat transfer augmentation [1–7]. One of the important porous media characteristics is represented by extensive contact surface between the solid and fluid which enhances the heat transfer area, interstitial heat transfer coefficient, and results in an increased thermal diffusivity.

A thorough understanding of the fluid mechanics and heat transfer characteristics in porous media is quite complicated. In this respect, the complex microscopic transport phenomena at the pore level is important since basically they result in such macroscopic phenomena as heat transfer augmentation and pressure loss increase. However, the complexity of the porous structure usually precludes a detailed microscopic investigation of the transport phenomena at the pore level. Therefore, the general transport equations are commonly integrated over a representative elementary volume, which accommodates the fluid and the solid phases within a porous structure. Though the loss of information with respect to the microscopic transport phenomena is inevitable with this approach, the integrated quantities, coupled with a set of proper constitutive equations which represent the effects of microscopic interactions on the integrated quantities, do provide a rigorous and effective basis for analyzing the transport phenomena in porous media.

Many studies in porous media are based on the use of Darcy flow model. In these works, various features of the momentum transport especially in the field of groundwater hydrology, petroleum reservoir and geothermal operations were investigated using this model [8, 9]. In some applications, however, non-Darcian effects are expected to become substantially more significant. In this regard, Vafai and Tien [10] have analyzed the effects of a solid boundary and the inertial forces and have provided insight on the applicability of the traditionally employed Darcy's law.

A more rigorous approach for investigating transport through porous media is through the use of the volume-averaging technique. There are two approaches available in applying the volume-averaging technique for heat transfer investigations: one is averaging over a representative elementary volume containing both the fluid and the solid phases, and the other is averaging separately over each of the phases, thus resulting in a separate energy equation for each individual phase. These two models are referred to as the one-equation model and the two-equation model, respectively.

The one-equation model is valid when the thermal communication is effective enough so that the local temperature difference is negligibly small between the fluid and the solid phases. This model has been utilized in various analysis of heat transfer in porous media [11–14]. While the one-equation model facilitates the heat transfer analysis, in some applications the temperature differences between phases cannot be neglected. In these situations the effects of the interfacial surface and the interstitial heat transfer coefficient, which are related to the internal heat exchange between the solid and fluid phases are major factors causing heat transfer augmentation in porous media. In such cases, the two-equation model needs to be utilized.

One of the early investigations based on a two-equation model was performed by Koh and Colony [15]. They used quite a restricted model which did not account for various important effects such as conduction through the fluid phase, dispersion and non-Darcian effects. Later on, Vafai and Sozen [16], and Amiri and co-workers [17, 18] investigated forced convective flow through porous media utilizing a rigorous formulation based on the locally volume averaged two-equation model. Their investigations provided detailed insight relative to momentum transport and thermal characteristics within porous media. Some additional aspects of the local thermal equilibrium have been presented by Whitaker [19] and Sozen and Vafai [20].

The main objective of this study is to present an analytical characterization, and conceptual assessment of solid and fluid temperature differentials in porous media. The applied model in this study incorporates the major characteristics of a porous medium such as the extensive interfacial area due to porous structures and the diffusion enhancement due to tortuous flow passages. Based on an exact solution, the heat transfer characteristics are classified into three regimes, and physical characteristics for each regime are analyzed. The Nusselt number at the channel wall is obtained as a function of the pertinent parameters. Another objective of the present work is to ascertain and explicitly specify conditions for which the

one-equation model would be applicable. To this end, the Nusselt number obtained from the two-equation model is compared with that from the one-equation model and a practical, criterion is prescribed for the validity of the one-equation model.

2. Problem description and modeling

The problem under investigation is related to forced convective flow through a channel filled with a porous medium as shown in Fig. 1. The height of the channel is $2H$ and a constant heat flux, q_w is applied to the channel wall. In analyzing the problem the following assumptions are invoked:

(1) Natural convection and radiative heat transfer are negligible;
(2) Variation of thermophysical properties with temperature is negligible;
(3) Flow and heat transfer in the channel are fully developed.

Based on these assumptions and for a constant heat flux boundary condition, the following set of governing equations is obtained from Amiri and Vafai [17] and Amiri et al. [18]:

Fluid phase

$$k_{f,eff}\nabla_y^2 T_f + h_i a(T_s - T_f) = \rho c_P u \frac{\partial T_f}{\partial x} \tag{1}$$

Solid phase

$$k_{s,eff}\nabla_y^2 T_s - h_i a(T_s - T_f) = 0 \tag{2}$$

where $k_{f,eff}$ and $k_{s,eff}$ are the effective fluid and solid thermal conductivities, respectively, T_f and T_s the fluid and solid temperatures, h_i the interstitial heat transfer coefficient, u the fluid velocity, ρ the density, c_P the specific heat of the fluid, and a is the interfacial area per unit volume of porous medium. The first term in each of the above equations represents the net transverse conduction and as such it can be written as

$$\nabla_y^2 T = \frac{\partial^2 T}{\partial y^2} \quad \text{or} \quad \nabla_y^2 T = \frac{1}{y}\frac{\partial}{\partial y}\left(y\frac{\partial T}{\partial y}\right) \tag{3}$$

where the first representation is used for a rectangular channel and the second representation is used for a circular cross section. The longitudinal conduction term is absent from the energy equations since the longitudinal conduction contribution to the net energy transfer is negligible for the thermally fully developed region with a constant wall heat flux boundary condition.

When a heat flux is directly applied to the outer surface of a porous medium, the applied heat is transferred to the solid and fluid parts. As noted in Amiri et al. [18], the wall heat flux boundary condition may be viewed in two different ways. The first is to assume that each representative elementary volume (which contains both fluid and solid phases) at the wall surface receives a prescribed heat flux that is equal to the wall heat flux q_w. As a result, the heat will be divided between the two phases on the basis of the physical values of their effective conductivities and their corresponding temperature gradients. The second approach is to assume that each of the individual phases at the wall surface will receive an equal amount of heat flux q_w.

However, a solid substrate of finite thickness and high thermal conductivity is usually attached to the porous medium as shown in Fig. 1, and the heat flux is applied to the outer wall of the substrate instead of being applied directly to the outer surface of the porous medium. In this case, the temperature at the interface between the porous medium and the solid substrate is likely to be uniform regardless of whether it contacts the solid or fluid due to the high thermal conductivity of the substrate. Therefore, the boundary condition when a high thermal conductivity substrate is present can be written as

$$T_f|_{y=H} \cong T_s|_{y=H} \cong T_w \tag{4}$$

where T_w implies the temperature at the interface. This temperature is not known a priori and must be obtained as a part of the solution. Consequently, one more equa-

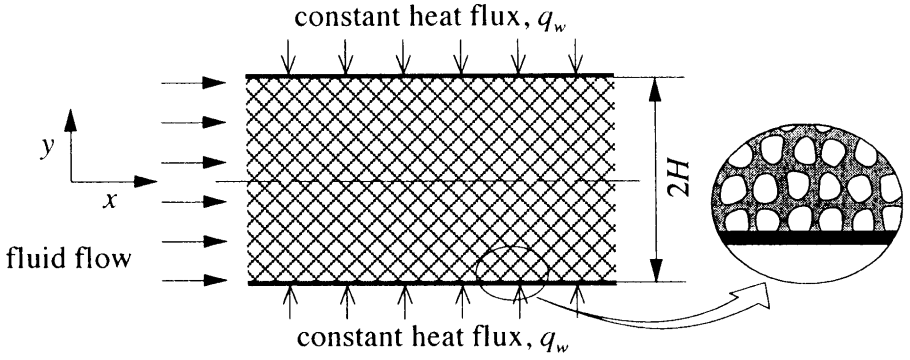

Fig. 1. Schematic diagram of the channel filled with a porous medium.

tion is required to complete the wall boundary condition. This additional equation is obtained from an energy balance at the interface as

$$q_w = k_{f,eff}\left.\frac{\partial T_f}{\partial y}\right|_{y=H} + k_{s,eff}\left.\frac{\partial T_s}{\partial y}\right|_{y=H}. \quad (5)$$

It should be noted that equation (5) is a similar representation of the first approach discussed earlier and cited in Amiri et al. [18]. The boundary condition at the center of the channel is standard and can be written as

$$\left.\frac{\partial T_f}{\partial y}\right|_{y=0} = \left.\frac{\partial T_s}{\partial y}\right|_{y=H} = 0. \quad (6)$$

The governing equations can be rendered dimensionless using the following nondimensional variables:

$$\theta = \gamma\frac{k_{s,eff}(T-T_w)/H}{q_w}, \quad \bar{u} = \frac{u}{\langle u\rangle}, \quad \eta = \frac{y}{H} \quad (7)$$

where $\langle\ \rangle$ designates the average over the channel cross section, and γ is the geometric constant defined by

$$\gamma = \frac{D}{4H} \quad (8)$$

in which D is the hydraulic diameter of the channel. The geometric constant, γ, depends on the geometry of the channel cross section. For example, it is 1 for a channel composed of parallel plates and 1/2 for circular channel.

Adding equations (1) and (2), and integrating it over the channel cross section and utilizing boundary conditions, equations (5) and (6), the integrated energy balance is obtained as

$$\rho c_p\left\langle u\frac{\partial T_f}{\partial x}\right\rangle = \rho c_p\langle u\rangle\frac{\partial T_f}{\partial x} = \frac{1}{\gamma H}q_w \quad (9)$$

In arriving at the above equation, it is assumed that the flow and heat transfer characteristics are hydrodynamically and thermally fully developed. Using equations (7)–(9), the governing equations (1) and (2) and boundary conditions given by equations (4) and (6) are nondimensionalized as

$$\kappa\nabla_\eta^2\theta_f + \frac{1}{\gamma}Bi(\theta_s-\theta_f) = \bar{u} \quad (10)$$

$$\nabla_\eta^2\theta_s - \frac{1}{\gamma}Bi(\theta_s-\theta_f) = 0 \quad (11)$$

$$\theta_s(1) = \theta_f(1) = 0 \quad (12)$$

$$\theta_s'(0) = \theta_f'(0) = 0 \quad (13)$$

where the two parameters, Bi and κ, are defined as

$$Bi = \frac{h_i\gamma aH^2}{k_{s,eff}}, \quad \kappa = \frac{k_{f,eff}}{k_{s,eff}}. \quad (14)$$

The parameter Bi is an equivalent Biot number representing the ratio of the conduction resistance in the solid phase to the thermal resistance associated with the internal convective heat exchange between the solid and fluid phases. The parameter κ represents the ratio of conduction resistances between the solid and fluid phases.

In what follows, the governing equations are solved for a channel flow between parallel plates and the pertinent heat transfer characteristics are discussed. In addition, the general characteristics of the heat transfer in a channel filled with porous media is addressed and physically distinct regimes are identified.

3. Heat transfer in a rectangular channel

The analytical solution is based on solving the coupled governing equations (10) and (11) along with the boundary conditions given by equations (12) and (13). The two coupled equations, each of which involves two unknown functions, θ_2 and θ_f, are manipulated to yield a new set of differential equations, each involving only one unknown function, i.e., either of θ_s or θ_f. The resultant equations become

$$\kappa\theta_s'''' - (1+\kappa)Bi\,\theta_f'' = -Bi \quad (15)$$

$$\kappa\theta_s'''' - (1+\kappa)Bi\,\theta_s'' = -Bi \quad (16)$$

where in the above equations the Darcian flow model has been utilized. Since these equations are fourth-order differential equations, two more boundary conditions are required for each equation in addition to the boundary conditions given by equations (12) and (13). A set of additional boundary conditions can be obtained by evaluating the second derivatives of θ_s and θ_f at the wall by utilizing equation (12) in equations (10) and (11). This results in

$$\theta_f''(1) = 1/\kappa, \quad \theta_s''(1) = 0. \quad (17)$$

The second set of additional boundary conditions is obtained by differentiating equations (10) and (11) with respect to η, evaluating them at $\eta = 0$ and utilizing equation (13). This results in the additional boundary conditions given by

$$\theta_f'''(0) = \theta_s'''(0) = 0. \quad (18)$$

The temperature distribution is now obtained by solving equations (15) and (16) along with the boundary conditions given in equations (12), (13), (17), and (18). Equations (15) and (16) are first integrated twice using the boundary conditions given by equations (17) and (18). This yields the second derivatives of temperature profiles θ_f'' and θ_s''. Integrating the expressions for θ_f'' and θ_s'' twice more with respect to η and using equations (12) and (13) yields the temperature profiles for the fluid and solid phases. The resultant equations are

$$\theta_f = \frac{1}{1+\kappa}\left[\frac{1}{2}(\eta^2-1) - \frac{1}{Bi(1+\kappa)}\left\{1-\frac{\cosh(\lambda\eta)}{\cosh(\lambda)}\right\}\right] \quad (19)$$

$$\theta_s = \frac{1}{1+\kappa}\left[\frac{1}{2}(\eta^2-1) - \frac{1}{Bi(1+\kappa)}\left\{1-\frac{\cosh(\lambda\eta)}{\cosh(\lambda)}\right\}\right] \quad (20)$$

where

$$\lambda = \sqrt{Bi(1+\kappa)/\kappa}. \tag{21}$$

Therefore, the temperature difference between the solid and fluid phases can be written as

$$\Delta\theta = \theta_s - \theta_f = \frac{1}{Bi(1+\kappa)}\left\{1 - \frac{\cosh(\lambda\eta)}{\cosh(\lambda)}\right\} \tag{22}$$

The Nusselt number based on the fluid temperature is a useful quantity that can be used for characterizing the heat transfer results. The wall heat transfer coefficient is defined by

$$h_w = \frac{q_w}{T_w - \langle T_f \rangle}. \tag{23}$$

Using equations (23), (7) and (14), Nusselt numbers based on the channel hydraulic diameter, D, and the effective fluid conductivity can be presented as

$$Nu_w = \frac{h_w D}{k_{f,eff}} = \frac{4\gamma^2}{\kappa(-\langle\theta_f\rangle)}. \tag{24}$$

The non-dimensionalized bulk mean temperature of the fluid, $\langle\theta_f\rangle$, can be obtained from equation (19) as

$$\langle\theta_f\rangle = -\frac{1}{1+\kappa}\left[\frac{1}{3} + \frac{1}{Bi(1+\kappa)}\left\{1 - \frac{1}{\lambda}\tanh(\lambda)\right\}\right]. \tag{25}$$

In arriving at equation (25), it is noted that the value of the geometric constant, γ, is 1 for a channel between parallel plates. Using equation (25) in the expression for the Nusselt number, Nu_w, given in equation (24) results in

$$Nu_w = 12\frac{1+\kappa}{\kappa}\frac{1}{1 + \dfrac{3}{Bi(1+\kappa)}\left\{1 - \dfrac{1}{\lambda}\tanh(\lambda)\right\}}. \tag{26}$$

The above expression describes the Nusselt number in terms of the ratio of the effective thermal conductivities, κ and the equivalent Biot number, Bi, given by equation (14).

4. Discussion of results

The temperature distribution for the fluid and solid phases for a range of parameters, Bi and κ are shown in Fig. 2. In this figure, the values of the key parameters, Bi and κ are chosen such that the influence of each parameter on the temperature profiles can be clearly illustrated. When the values for Bi and κ are both small as in Fig. 2(a), the temperature difference between the solid and fluid phases is relatively large and the temperature distribution is nearly uniform over the core part of the channel. This is due to the small equivalent Biot number, Bi, which translates into a small heat transfer coefficient, h_i, for the internal heat exchange and the fluid conduction being confined to a region near the wall due to a relatively small fluid conductivity. As the Biot number increases, the temperature difference becomes smaller while the solid temperature hardly changes as shown in Fig. 2(b). The temperature difference is also early uniform in this case due to the relatively small fluid conductivity.

For larger values of both parameters, Bi and κ, the temperature profiles are shown in Fig. 2(c). It is seen that the solid temperature profile is similar to that shown in Fig. 2(b), though the scale is two orders of magnitude different. It is worth noting that the fluid temperature profile is parabolic, which implies that the influence of the fluid conduction prevails over most of the channel cross section instead of being confined in a narrow region near the wall as was the case for Bi and κ values corresponding to Fig. 2(a) or (b). This is due to the relatively larger fluid conductivity utilized in producing Fig. 2(c). A decrease in the Biot number, as compared to the value used in Fig. 2(c), results in an increase in the temperature differential while the fluid temperature is hardly affected as can be seen in Fig. 2(d). This is because the fluid conduction dominates the heat transfer process in the porous medium in both cases shown in Fig. 2(c) and (d), and the solid temperature is much more influenced by the degree of the internal heat exchange between the fluid and solid phases rather than influenced by its own conductivity.

The Nusselt number variations as a function of the key physical parameters, Bi and κ, is displayed in Fig. 3. The three-dimensional plot shown in Fig. 3 is based on equation (26). This figure reveals the existence of three distinct regimes, each of which appears as a tangential plane. The occurrence of the three regimes is also evidenced in Fig. 4, which is basically a top view of Fig. 3. The heat transfer characteristics pertinent to each regime are substantially different from each other. For convenience, these regimes are referred to as Regimes I, II and III, as shown in Fig. 4.

The asymptotic behavior of the Nusselt number in each regime is obtained using the following asymptotic relation:

$$\frac{1}{\lambda}\tanh(\lambda) \approx \begin{cases} 1-\lambda^2/3 & \text{as}\lambda \to 0 \\ 1/\lambda & \text{as } \lambda \to \infty \end{cases}. \tag{27}$$

When $\lambda \to 0$, the asymptotic behavior of the Nusselt number can be obtained from equations (26) and (27) as

$$Nu_w \to 12. \tag{28}$$

Based on the definition of λ, given in equation (21), the condition, $\lambda \to 0$ can be rewritten as

$$Bi \ll \frac{\kappa}{1+\kappa}. \tag{29}$$

Equation (29) is satisfied within Regime 1 displayed in Fig. 4. On the other hand, when $\lambda \to \infty$, the Nusselt number becomes

$$Nu_w \approx 12\frac{1+\kappa}{\kappa}\frac{1}{1 + \dfrac{3}{Bi(1+\kappa)}}. \tag{30}$$

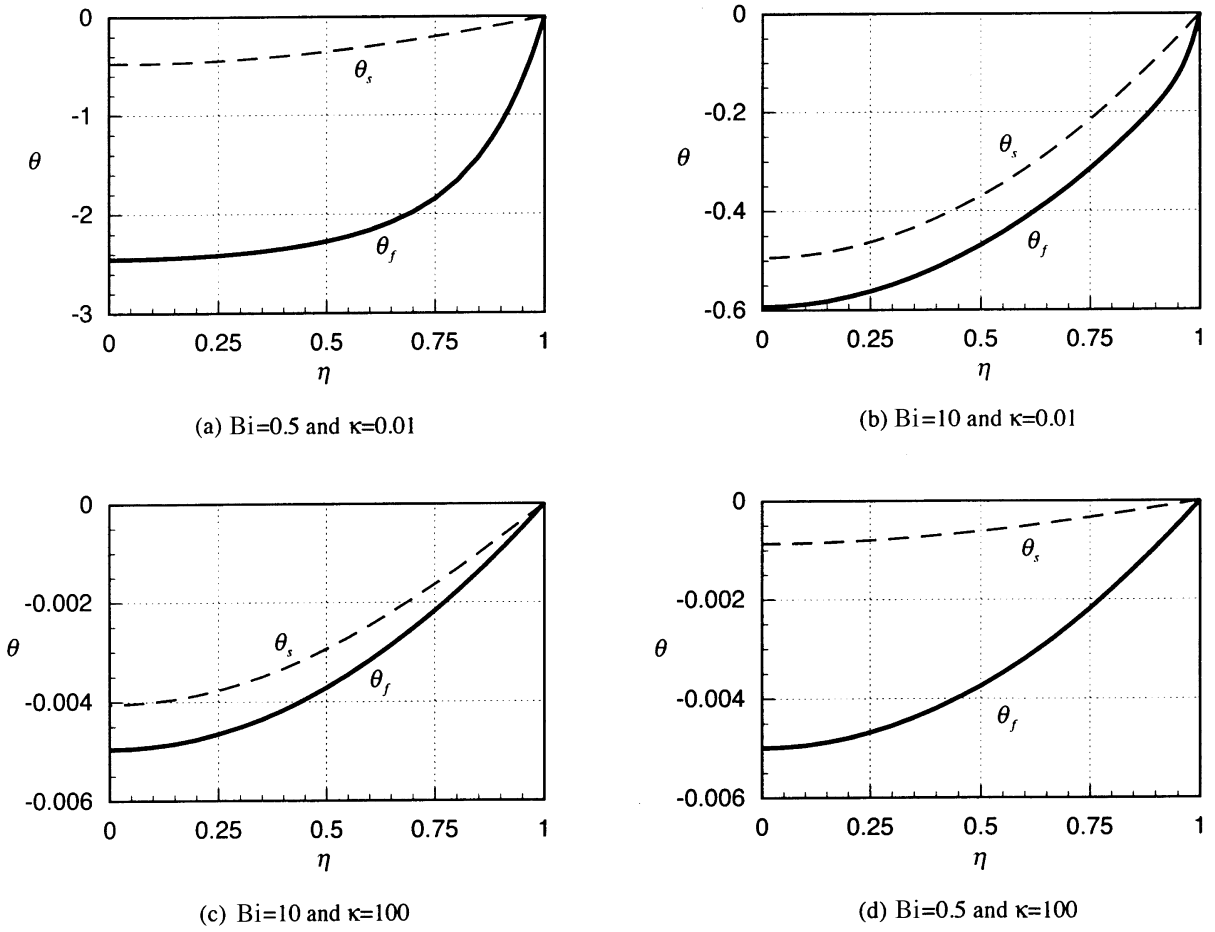

Fig. 2. Temperature profiles for both fluid and solid phases: (a) $Bi = 0.5$ and $\kappa = 0.01$; (b) $Bi = 10$ and $\kappa = 0.01$; (c) $Bi = 10$ and $\kappa = 100$; (d) $Bi = 0.5$ and $\kappa = 100$.

This equation can be subdivided into three regimes depending on the corresponding magnitudes of the physical parameters, Bi and κ. First, it should be noted that when $Bi \to \infty$ and $\kappa \to \infty$, the Nusselt number converges to a constant value, i.e.

$$Nu_w \to 12. \tag{31}$$

This regime essentially collapses to what has already been established as Regime I. Next, it should be noted that when $Bi \to \infty$ and $\kappa \to 0$, the Nusselt number becomes

$$Nu_w \approx 12\frac{1}{\kappa}. \tag{32}$$

This constitutes the second regime (Regime II) as displayed in Fig. 4. Finally, when $Bi \to 0$ and $\kappa \to 0$, the Nusselt number can be approximated from equation (30) as

$$Nu_w \approx 4\frac{Bi}{\kappa}. \tag{33}$$

This constitutes the third regime (Regime III) as shown in Fig. 4.

5. Physical interpretation of different regimes

In this section, the physical aspects of the three different regimes and the heat transfer processes associated with each one are examined. It should be emphasized that the following discussion is not confined to a channel with a rectangular cross section, rather the results cover the general features of the heat transfer in a channel with an arbitrary cross section filled with a porous medium. To this end, the relevant heat transfer processes are illustrated in Fig. 5 together with typical temperature profiles for the solid and fluid phases. For the problem description presented in Section 2 and shown in Fig. 5, the heat flux, q_w, from the outer surface can be considered to be

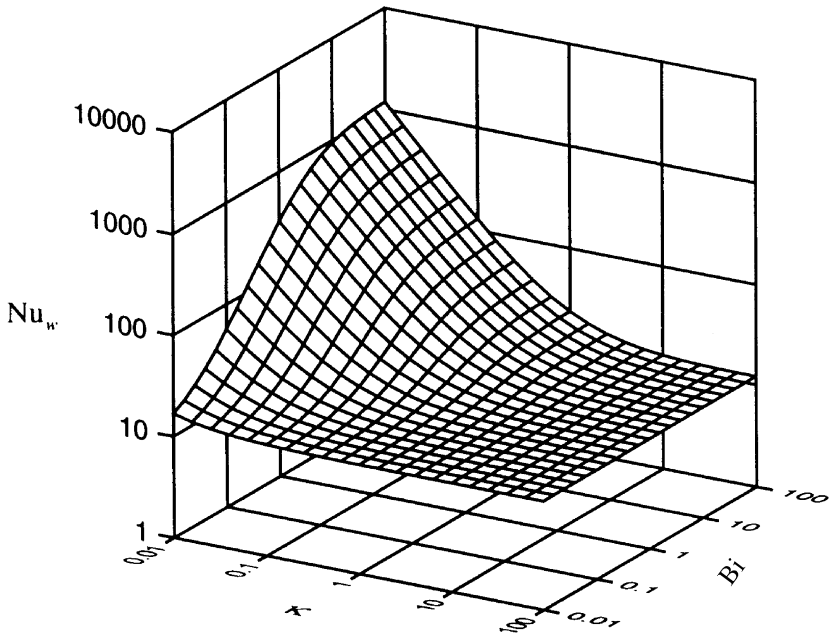

Fig. 3. Nusselt number variations as a function of the key physical parameters, *Bi* and κ.

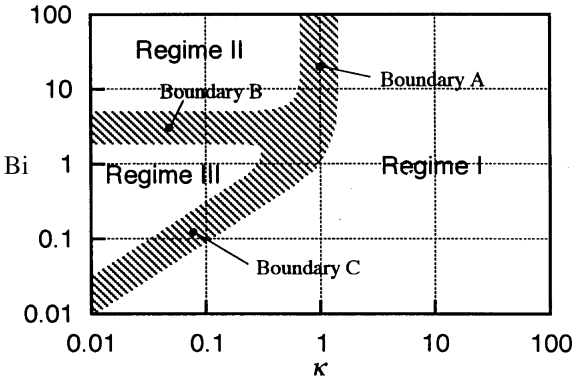

Fig. 4. Base projection of Fig. 3 displaying three physically relevant regimes.

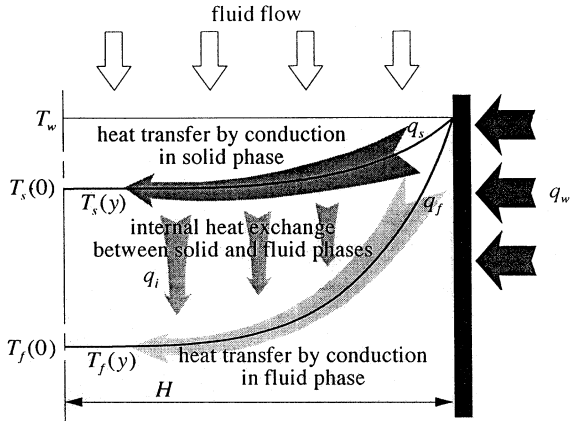

Fig. 5. Schematic of the physical aspects of the heat transfer process in porous media.

transferred into the porous medium in two ways: one is conduction in the fluid phase and the other is conduction in the solid phase. The sum of the heat transferred by the fluid conduction, q_f, and that by the solid conduction, q_s, equals the total wall heat flux, q_w. That is

$$q_w = q_f + q_s. \tag{34}$$

This methodology is consistent with the first approach outlined by Amiri et al. [18]. The heat transferred into the solid phase is ultimately transferred to the fluid phase through the internal heat exchange process. Accordingly, the total internal heat exchange equals to the total heat transferred from the wall to the solid phase via solid conduction. That is

$$q_i = q_s. \tag{35}$$

The overall heat transfer to the fluid phase is partly by direct conduction into the fluid as well as by conduction through the solid and subsequent internal heat exchange from the solid to the fluid, which is eventually convected out of the porous medium by the flow.

Based on the above description and Fig. 5, it can be stated that there are three distinct processes involved in

heat transfer through a porous medium. Each of the cited heat transfer processes can be written in terms of a thermal resistance and a relevant temperature potential as

$$q_f = \frac{T_w - T_f(0)}{R_f}, \quad q_s = \frac{T_w - T_s(0)}{R_s}, \quad q_i = \frac{T_s(0) - T_f(0)}{R_i} \tag{36}$$

where R_f, R_s, and R_i are the thermal resistance related to the fluid conduction, solid conduction and internal heat exchange, respectively. The temperature potential is chosen so that it will correspond to the largest temperature difference associated with each of the heat transfer processes. The overall heat transfer can be written as

$$q_w = \frac{T_w - T_f(0)}{R_o} \tag{37}$$

where R_o represents the overall thermal resistance of the porous medium.

The thermal resistances can be obtained by writing the relevant heat fluxes in an alternative form as

$$q_f = k_{f,eff} \left.\frac{\partial T_f}{\partial y}\right|_{y=H}, \quad q_s = k_{s,eff} \left.\frac{\partial T_s}{\partial y}\right|_{y=H},$$
$$q_i = h_i A_i (\langle T_s \rangle - \langle T_f \rangle)/A_w \tag{38}$$

where A_i is the interfacial area between the solid and fluid phases and A_w is the surface area of the porous medium in contact with the channel wall. Equating the corresponding terms in equations (36) and (38) results in the three pertinent thermal resistances which are involved in transport process through porous media. These are

$$R_f = c_f \frac{H}{k_{f,eff}}, \quad R_s = c_s \frac{H}{k_{s,eff}}, \quad R_i = c_i \frac{A_w}{h_i A_i} \tag{39}$$

where cs are the proportionality constants defined by

$$c_f = -\frac{\theta_f(0)}{\theta_f'(1)}, \quad c_s = -\frac{\theta_s(0)}{\theta_s'(1)}, \quad c_i = \frac{\Delta\theta(0)}{\langle \Delta\theta \rangle}. \tag{40}$$

The area ratio, A_i/A_w, in equation (39) represents the surface extension due to the porous medium insertion, and can be written for a channel with a uniform cross section area as

$$\frac{A_i}{A_w} = a\frac{V}{A_w} = a\frac{A_c}{P} = a\gamma H \tag{41}$$

where A_c is the cross section area and P is the perimeter of the channel. The proportionality constants, cs depend on the temperature profiles at a cross section and thus reflect the flow passage geometry which is typically either composed of two parallel plates, a circular pipe, a rectangular duct, or an annulus. For example, for a parabolic temperature profile such as that for a flow between parallel plates, the proportionality constants are evaluated as

$$c_f = \tfrac{1}{2}, \quad c_s = \tfrac{1}{2}, \quad c_i = \tfrac{3}{2} \tag{42}$$

while these constants for a circular cross section are

$$c_f = \tfrac{1}{2}, \quad c_s = \tfrac{1}{2}, \quad c_i = 2. \tag{43}$$

It should be noted that each of the three thermal resistances given in equation (39) is based on a different set of parameters.

the total thermal resistance of the porous medium can be evaluated from equations (34)–(37) as

$$\frac{1}{R_o} = \frac{1}{R_f} + \frac{1}{R_s + R_i}. \tag{44}$$

The above equation shows that the solid conduction resistance and the internal exchange resistance are connected in series resulting in $R_s + R_i$ as the total thermal resistance of the solid phase, while the fluid conduction resistance is connected in parallel to the thermal resistance of the solid phase and the internal exchange resistance to give the overall thermal resistance of the porous media. The electrical analogy for heat transfer in porous media based on equation (44) is shown in Fig. 6. This figure illustrates how the three thermal resistances are mutually connected and how the total thermal resistance is determined from the three thermal resistances.

In a parallel electrical circuit, most of the electric current flows through the smallest resistance among otheres, and thus the circuit is mainly governed by the smallest resistance. In the same manner the overall heat transfer in porous media will be dominated by the thermal resistance which affects the overall thermal resistance the most. Since each of the three thermal resistances is physically distinct, the resulting heat transfer process will display distinctive characteristics depending on the dominating thermal resistance. Consequently, the existence of three distinguished heat transfer regimes can be expected based on physical mechanisms displayed in Figs 5 and 6. Furthermore, an important one to one connection will be established between the thermal resistance network and the three regime map shown in Fig. 4.

The three regimes shown in Fig. 4 are re-established through a comparative analysis of the three resistances shown in Fig. 6. Specifically, the three regimes shown in Fig. 4 are reconfirmed as

Regime I: when R_f is dominant where $R_f \ll R_i$ or $R_f \ll R_s$
Regime II: when R_s is dominant where $R_s \gg R_i$ and $R_s \ll R_f$
Regime III: when R_i is dominant where $R_i \gg R_s$ and $R_i \ll R_f$.

These three regimes are identified by the three boundaries separating each of the regimes, i.e., $R_f \approx R_s$, $R_s \approx R_i$, and $R_i \approx R_f$. Each of three boundaries can be written in terms of the parameters, Bi and κ using equations (39), (40), (41), and (14):

Boundary A (between Regime I and Regime II):

$$R_f \approx R_s \to \kappa \approx \frac{\theta_f(0)}{\theta_f'(1)} \frac{\theta_s'(1)}{\theta_s(0)}. \tag{45}$$

Boundary B (between Regime II and Regime III):

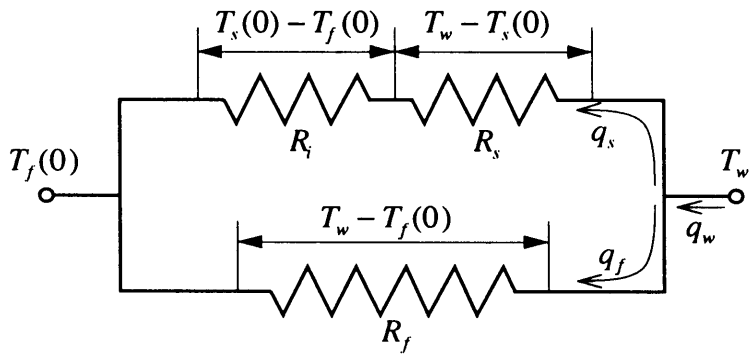

Fig. 6. Electrical analogy for the heat transfer process in porous media.

$$R_s \approx R_i \to Bi \approx \frac{-\Delta\theta(0)}{\langle\Delta\theta\rangle}\frac{\theta_s'(1)}{\theta_s(0)}. \tag{46}$$

Boundary C (between Regime III and Regime I):

$$R_i \approx R_f \to \frac{Bi}{\kappa} \approx -\frac{\Delta\theta(0)}{\langle\Delta\theta\rangle}\frac{\theta_f'(1)}{\theta_f(0)}. \tag{47}$$

At boundary A, between Regime I and Regime II, the fluid and the solid conduction resistances are of the same order of magnitude, and the internal exchange resistance is the smallest among the three thermal resistances. Due to the small internal exchange resistance, the temperature difference between the fluid and solid phase becomes negligible, and thus the temperature profiles for the fluid and solid become similar to each other. Consequently, based on equation (45), this boundary can be characterized by

$$\kappa \approx 1. \tag{48}$$

The boundary between Regimes II and III is characterized by a solid conduction resistance which is of the same order of magnitude as the internal exchange resistance, while the fluid conduction resistance is the largest among the three resistances. Due to the large conduction resistance in the fluid phase, the energy from the wall is hardly transferred directly into the fluid. Therefore, the fluid conduction contribution in equation (10) is negligible causing the temperature difference between the fluid and solid to become nearly uniform over the channel cross section. As a result, the solid temperature profile can be readily obtained from equation (11) for a fixed and known temperature difference, which can directly be evaluated from equation (10). Thus, based on equation (46), the boundary B, between Regimes II and III can be described by

$$Bi \approx -\frac{\theta_s'(1)}{\theta_s(0)} \equiv c_1. \tag{49}$$

At boundary C, the internal resistance and the fluid conduction resistance are similar in magnitude and the solid conduction resistance is the smallest. It should be noted that even though the solid conduction resistance can be significant over portions of Regime I, it is quite small at boundary C which is the portion in common between Regimes III and I. Hence the solid temperature becomes quite close to the wall temperature and thus the temperature difference profile, $\Delta\theta$, is nearly the same as that of the fluid temperature, θ_f. Consequently based on equation (47), boundary C can be rewritten as

$$\frac{Bi}{\kappa} \approx -\frac{\theta_f'(1)}{\langle\theta_f\rangle} \equiv c_2. \tag{50}$$

The fluid temperature profile at this boundary can be obtained from equation (10) by letting θ_s equal zero.

In equations (49) and (50), the constants, c_1 and c_2, are determined from the temperature profiles. Each of these constants is of the order of magnitude of one at each boundary, since either the solid conduction or the fluid conduction prevails across the cross sectional area of the channel. In particular, for a uniform flow in a channel between parallel plates, the constants are evaluated as

$$c_1 = 2, \quad c_2 = 3.67 \tag{51}$$

while these constants for a circular cross section are

$$c_1 = 2, \quad c_2 = 5.53. \tag{52}$$

Comparing the boundaries given by equations (48)–(51) with those shown in Fig. 4, reveals that they are in exact agreement, and thus the Regimes I, II, and III in Fig. 4 are the same as those presented in connection with Fig. 6. Therefore, the three regimes shown in Fig. 4 are formed due to the existence of three distinct thermal resistances, and each regime shown in Fig. 4 is dominated by one of the three thermal resistances. Based on this observation, the heat transfer process within each regime can be viewed in terms of a dominating thermal resistance.

6. Heat transfer characterization within each regime

The original governing equations can be reduced to simpler forms by considering the magnitudes of the par-

Table 1.
Heat transfer characteristics within each regime

	Dominant thermal resistance	Range [obtained from equations (48)–(50)]	Reduced governing equations [obtained from equations (10) and (11)]	Nusselt number, Nu_w [obtained from equation (55)]	Heat transfer coefficient, $h_w = Nu_w k_{f,eff}/D$ [obtained from equations (55), (8) and (14)]
Regime I	R_f	$\kappa \gg 1$ or $Bi/\kappa \ll c_2$†	$\kappa\nabla_\eta^2\theta_f \approx \bar{u}$ $\nabla_\eta^2\theta_s - Bi\theta_s = -Bi\theta_f$	$-4\gamma\dfrac{\theta_f'(1)}{\langle\theta_f\rangle}$	$-\dfrac{\theta_f'(1)}{\langle\theta_f\rangle}\dfrac{k_{f,eff}}{H}$
Regime II	R_s	$Bi \gg c_1$* and $\kappa \ll 1$	$\theta_f \approx \theta_s - \bar{u}/Bi \approx \theta_s$ $\nabla_\eta^2\theta_s \approx \bar{u}$	$-4\gamma\dfrac{\theta_s'(1)}{\langle\theta_s\rangle}\dfrac{1}{\kappa}$	$-\dfrac{\theta_s'(1)}{\langle\theta_s\rangle}\dfrac{k_{s,eff}}{H}$
Regime III	R_i	$Bi \ll c_1$ and $Bi/\kappa \gg c_2$	$\theta_f \approx \theta_s - \bar{u}/Bi \approx -\bar{u}/Bi$ $\nabla_\eta^2\theta_s \approx \bar{u}$	$4\gamma^2\dfrac{Bi}{\kappa}$	$\gamma a H h_i$

* c_1 and c_2 are constants which depend on the geometry of the channel cross-section.

ameters, Bi and κ which in turn specifies the dominant thermal resistance within each regime. These equations and the relevant resistances which are summarized in Table 1 provide a clear, physical view of the heat transfer process in porous media. The range within each regime is obtained by observing the boundaries A, B, C given in equations (45)–(47) and equations (48)–(50).

For example, when $\kappa \gg 1$ in Regime I, the governing equation obtained by summing equations (10) and (11) is reduced to

$$\kappa\nabla_\eta^2\theta_f \approx \bar{u} \tag{53}$$

because κ is much larger than unity in this regime. On the other hand, if $Bi/\kappa \ll c_2$ in Regime I, the governing equation (10) is directly reduced to equation (53). This reduced governing equation implies that the fluid conduction is in balance with convection, while the solid conduction contribution is negligible compared to that from fluid conduction.

However, the solid conduction term is comparable to the convection term in Regimes II and III since the solid conductivity is much larger than the fluid conductivity in these regimes. It should be noted that the fluid conduction still dominates in the regime, $Bi/\kappa \ll c_2$ and $\kappa \ll 1$, which belongs to Regime I, even though the solid conductivity is much larger than that of the fluid. This is because the heat from the wall can hardly transfer through the solid phase in spite of the large solid conductivity due to the large internal heat exchange resistance between the solid and fluid phases. Consequently, most of the heat flows directly into the fluid and thus the fluid conductivity dominates the overall heat transfer in this regime.

The Nusselt number can be written in terms of the overall thermal resistance using equations (23), (24), and (37), as

$$Nu_w = \frac{\theta_f(0)}{\langle\theta_f\rangle}\frac{D/k_{f,eff}}{R_o}. \tag{54}$$

Since in each regime, the overall thermal resistance, R_o, can be approximated as R_f, R_s, or R_i, the Nusselt number in each regime can be written by using equations (39)–(41) and equation (8) as

$$\begin{aligned}
&\text{Regime I} \quad Nu_w \approx -4\gamma\frac{\theta_f'(1)}{\langle\theta_f\rangle}\\
&\text{Regime II} \quad Nu_w \approx -4\gamma\frac{\theta_f(0)}{\langle\theta_f\rangle}\frac{\theta_s'(1)}{\theta_s(0)}\frac{1}{\kappa}\\
&\text{Regime III} \quad Nu_w \approx 4\gamma\frac{\theta_f(0)}{\langle\theta_f\rangle}\frac{\langle\Delta\theta\rangle}{\Delta\theta(0)}\frac{Bi}{\kappa}.
\end{aligned} \tag{55}$$

The Nusselt numbers given by equation (55) can be further simplified by observing the reduced governing equations given in Table 1 and assessing the fluid and solid temperature profiles based on the reduced governing equations given in the same table. Specifically, the Nu_w in Regime II is reduced by noting from the reduced form of equations (10) and (11) given in Table 1 that $\theta_f \approx \theta_s$. Likewise, Nu_w in Regime III is reduced by observing from the reduced form of equations (10) and (11) that both θ_f and $(\theta_s - \theta_f)$ are essentially constants across the flow cross section. The resulting Nusselt number in each regime is summarized in Table 1 together with the pertinent wall heat transfer coefficients, h_w. The Nusselt numbers in Regimes I and II are shown to be dependent on the temperature profiles of the fluid and solid phases, respectively. This is because either the fluid or the solid conduction dominates the overall heat transfer in each regime. On the other hand, in the third regime (Regime III), heat transfer is dominated by the internal exchange resistance and as such, the Nusselt number is not influenced by either the fluid or the solid temperature profiles.

For the case of a uniform flow between parallel plates, the Nusselt number in each regime is evaluated from the reduced governing equations given in Table 1, as

$$Nu_w \approx \begin{cases} 12 & \text{in Regime I} \\ 12/\kappa & \text{in Regime II} \\ 4B/\kappa & \text{in Regime III} \end{cases}. \quad (56)$$

It should be noted that these values are the same as those from the analytical solution given in equations (28), (32) and (33).

It is worth noting the magnitude of the heat transfer coefficient for Regime III. As given in Table 1, the ratio of the wall heat transfer coefficient, h_w, to the internal heat exchange coefficient, h_i, is

$$\frac{h_w}{h_i} \approx \gamma a H. \quad (57)$$

Using equation (41), equation (57) can be rewritten as

$$\frac{h_w}{h_i} \approx \frac{A_i}{A_w}. \quad (58)$$

This equation clearly shows that the heat transfer enhancement due to the presence of a porous medium is directly proportional to the ratio of the surface enhancement (interfacial area between solid and fluid phases) so that of the outer surface area of the porous medium. Essentially, this feature in Regime III is the result of an internal exchange resistance which is larger than the solid conduction resistance as well as a temperature difference between the wall and solid phase which is negligibly small compared to that between the solid and fluid phases.

7. Criterion for validity of the one-equation model

In this part, the validity of the one-equation model is investigated by comparing the Nusselt number obtained from the one-equation model with that previously obtained from the two-equation model. In the one-equation model, the governing equation can be obtained from equations (10) and (11) by adding them and assuming the temperatures of the fluid and solid phases are the same. This leads to

$$(\kappa+1)\nabla_\eta^2\theta = \bar{u}. \quad (59)$$

The relevant boundary conditions are

$$\theta'(0) = 0 \quad \text{and} \quad \theta(1) = 0. \quad (60)$$

The temperature profile for a uniform flow in a channel between parallel plates can be readily obtained as

$$\theta = \frac{1}{2(1+\kappa)}(\eta^2 - 1). \quad (61)$$

With this temperature profile, the Nusselt number is obtained from equation (24) as

$$Nu_{w1} = 12\frac{1+\kappa}{\kappa}. \quad (62)$$

where the subscript '1' in Nu_{w1} emphasizes the point regarding the use of the one-equation model in obtaining the Nusselt number given by equation (62). The difference between the one-equation and two-equation model Nusselt numbers can now be evaluated through the use of equations (26) and (62). This results in

$$E \equiv \frac{Nu_{w1} - Nu_w}{Nu_w} = \frac{3}{Bi(1+\kappa)}\left\{1 - \frac{1}{\lambda}\tanh(\lambda)\right\}. \quad (63)$$

Figure 7 shows the contour error map in obtaining the Nusselt number based on the one-equation model as given by the equation (63). The error in using the one-equation model is found to increase as both parameters, Bi and κ become smaller, while the error in using the one-equation model decreases as either one of the parameters becomes larger. Since the temperature difference between the solid and fluid phases becomes smaller with an increase in the Biot number, it can be seen why the error in using the one-equation model decreases when the Biot number increases.

It is important to note that the result from the one-equation model is valid when the conductivity ratio, κ, is large regardless of the magnitude of the Biot number as seen in Fig. 7. This is due to a dominant fluid conduction relative to a negligible solid phase conduction in porous media when the conductivity ratio is large. Subsequently, even though the temperature difference is not small between the solid and fluid phases, the heat transfer process can be accurately presented by a one-equation model.

While the two-equation model is always more accurate than the one-equation model, in general, the two-equation model is more involved due to the inherent coupling of the solid and fluid phases. Analyzing the limiting behavior of equation (63) when $\kappa \to 0$ and when $Bi \to 0$ with the use of equation (27), and referring to Fig. 7, the

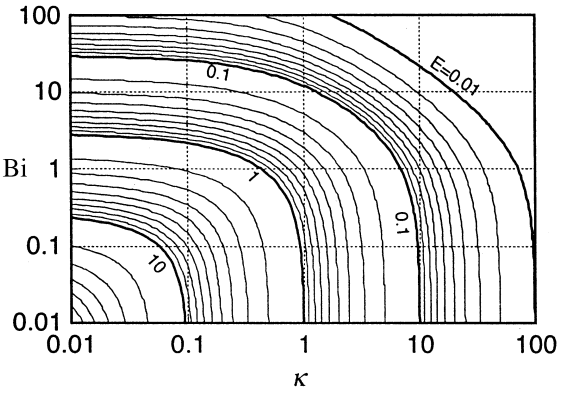

Fig. 7. Error map for the Nusselt number based on using the one-equation model.

criterion for the validity of the one-equation model can be written as

$$\kappa + \frac{Bi}{4} > \frac{1}{E_a}. \tag{64}$$

for a channel between parallel plates, where E_a is the allowable error in using the one-equation model. For a circular cross section this criterion is given as

$$\kappa + \frac{Bi}{4} > \frac{1}{E_a}. \tag{65}$$

Specifically, this criterion represents the region within which the error in the Nusselt number based on the one-equation model is less than or equal to E_u. Unless this criterion within the region of interest is satisfied, the two-equation model needs to be applied to stay within an error bound of E_u.

8. Conclusions

A theoretical investigation of the heat transfer characteristics for the forced convective flow through a channel filled with porous material is presented in this work. To this end, exact solutions are obtained for both the fluid and solid temperature fields based on the two-equation model including transverse conduction contributions. Utilizing the exact solution, the Nusselt number is obtained as a function of two pertinent parameters, i.e., the Biot number, Bi, and the ratio of effective conductivities between the fluid and solid phases, κ. It is shown that the heat transfer characteristics in porous media can be classified into three regimes, each of which is dominated by one of three distinctive heat transfer mechanisms, i.e., fluid conduction, solid conduction, and internal heat exchange between the fluid and solid phases. These three distinct regimes represent the physical aspects of heat transfer in porous media and are characterized as follows:

Regime I ($\kappa \gg 1$ or $Bi/\kappa \ll c_2$)—Fluid conduction dominates the heat transfer process in porous media while the solid phase does not contribute directly to the overall heat transfer. The wall heat transfer coefficient depends on the effective fluid thermal conductivity.

Regime II ($Bi \gg c_1$ and $\kappa \ll 1$)—Solid conduction dominates the heat transfer and the temperature difference between phases is negligible due to the relatively large interstitial heat transfer coefficient. The effective solid thermal conductivity determines the wall heat transfer coefficient.

Regime III ($Bi \ll c_1$ and $Bi/\kappa \gg c_2$)—Internal heat exchange dominates the heat transfer. The solid temperature is almost the same as the wall temperature due to the relatively large solid conductivity and thus the porous structure works as an ideal fin system. The wall heat transfer coefficient is determined by the interstitial heat transfer coefficient and the specific interfacial area.

In the cited classifications, c_1 and c_2 are constants of the order of 1 which depend on the channel cross sectional geometry. The validity of the one-equation model is also investigated by comparing the Nusselt number obtained from the one-equation model with that from the two-equation model. The error in using the one-equation model is found to increase as both of the parameters, Bi and κ become smaller, thus causing the one-equation model invalid.

Acknowledgement

The support provided by KIST during Dr D. Y. Lee's stay at The Ohio State University is acknowledged and appreciated.

References

[1] J.C.Y. Koh, R.L. Stevens, Enhancement of cooling effectiveness by porous materials in coolant passage, J. Heat Transfer 97 (1975) 309–311.
[2] T.M. Kuzay, J.T. Collins, A.M. Khounsary, G. Morales, Enhanced heat transfer with metal-wood-filled tubes, Proc. of ASME/JSEM Thermal Eng. Conf. 1991, pp. 145–151.
[3] P.C. Huang, K. Vafai, Flow and heat transfer control over an external surface using a porous block array arrangement, Int. J. Heat Mass Transfer 36 (1993) 4019–4032.
[4] K. Vafai, P.C. Huang, Analysis of heat transfer regulation and modification employing intermittently emplaced porous cavities, J. Heat Transfer 116 (1994) 604–613.
[5] P.C. Huang, K. Vafai, Analysis of forced convection enhancement in a channel using porous blocks, J. Thermophysics and Heat Transfer 8 (1994) 563–573.
[6] J.H. Rosenfeld, M.T. North, Porous media heat exchangers for cooling of high-power optical components, Optical Engineering 34 (1995) 335–341.
[7] M.G. Izenson, J.L. Martin, Optimal thermal-hydraulic performance for helium cooled divertors, Fusion Technology 29 (1996) 545–558.
[8] M.A. Combarnous, S. A. Bories, Hydrothermal convection in saturated porous media, Advances in Hydroscience 10 (1975) 231–307.
[9] P. Cheng, Heat transfer in geothermal systems, Advances in Heat Transfer 14 (1978) 1–105.
[10] K. Vafai, C.L. Tien, Boundary and inertia effects on flow and heat transfer in porous media, Int. J. Heat Mass Transfer 24 (1981) 195–203.
[11] R. Siegel, M.E. Goldstein, Theory of heat transfer in a two-dimensional porous cooled medium and application to an eccentric annular region, J. Heat Transfer 94 (1972) 425–431.
[12] D. Poulikakos, K. Renken, Forced convection in a channel filled with porous medium, including the effects of flow inertia, variable porosity, and Brinkman friction, J. Heat Transfer 109 (1987) 880–888.

[13] M.L. Hunt, C.L. Tien, Effects of thermal dispersion on forced convection in fibrous media, Int. J. Heat Mass Transfer 31 (1988) 301–309.
[14] K. Vafai, S.J. Kim, Forced convection in a channel filled with a porous medium: an exact solution, J. Heat Transfer 111 (1989) 1103–1106.
[15] J.C.Y. Koh, R. Colony, Analysis of cooling effectiveness for porous material in a coolant passage, J. Heat Transfer 96 (1974) 324–330.
[16] K. Vafai, M. Sozen, Analysis of energy and momentum transport for fluid flow through a porous bed, J. Heat Transfer 112 (1990) 690–699.
[17] A. Amiri, K. Vafai, Analysis of dispersion effects and non-thermal equilibrium, non-Darcian, variable porosity incompressible flow through porous media, Int. J. Heat Mass Transfer 37 (1994) 939–954.
[18] A. Amiri, K. Vafai, T.M. Kuzay, Effects of boundary conditions on non-Darcian heat transfer through porous media and experimental comparisons, Numerical Heat Transfer, Part A (1995) 651–664.
[19] S. Whitaker, Simultaneous heat, mass and momentum transfer in porous media: a theory of drying, Advances in Heat Transfer 13 (1977) 119–203.
[20] M. Sozen, K. Vafai, Analysis of oscillating compressible flow through a packed bed, International Journal of Heat and Fluid Flow 12 (1991) 130–136.